Journal of Materials Chemistry A

Iodine-rich mixed composition perovskites optimised for tin(IV) oxide transport layers: The influence of halide ion ratio, annealing time, and ambient air aging on solar cell performance

Journal:	*Journal of Materials Chemistry A*
Manuscript ID	TA-ART-02-2019-002142.R2
Article Type:	Paper
Date Submitted by the Author:	08-Jun-2019
Complete List of Authors:	Ozaki, Masashi; Kyoto University, Institute for Chemical Research Ishikura, Yasuhisa; Kyoto University, Institute for Chemical Research Truong, Minh Anh ; Kyoto University, Institute for Chemical Research Liu, Jiewei; Kyoto University, Institute for Chemical Research Okada, Iku; Tokyo Chemical Industry Co Ltd, Toda Research Center Tanabe, Taro; Tokyo Chemical Industry Co Ltd, Toda Research Center Sekimoto, Shun; Kyoto University, Institute for Integrated Radiation and Nuclear Science Ohtsuki, Tsutomu ; Kyoto University, Institute for Integrated Radiation and Nuclear Science Murata, Yasujiro; Kyoto University, Institute for Chemical Research Murdey, Richard; Kyoto University, Institute for Chemical Research Wakamiya, Atsushi; Kyoto University, Institute for Chemical Research

ARTICLE

Received 00th January 20xx,
Accepted 00th January 20xx

DOI: 10.1039/x0xx00000x

Iodine-rich mixed composition perovskites optimised for tin(IV) oxide transport layers: The influence of halide ion ratio, annealing time, and ambient air aging on solar cell performance

Masashi Ozaki,[a] Yasuhisa Ishikura,[a] Minh Anh Truong,[a] Jiewei Liu,[a] Iku Okada,[b] Taro Tanabe,[b] Shun Sekimoto,[c] Tsutomu Ohtsuki,[c] Yasujiro Murata,[a] Richard Murdey[a] and Atsushi Wakamiya*[a]

Iodine-rich mixed composition metal-halide perovskites were developed to improve the performance of perovskite solar cell devices incorporating tin(IV) oxide substrates for electron transport layers by optimizing the I/Br halide ion ratio. Device performance was further enhanced by exposing to ambient atmosphere over several days, which correlated with a shift of the energy levels in the perovskite and significant suppression of charge carrier recombination. A high power conversion efficiency of 20.6% was obtained for the aged device.

Introduction

Metal halide perovskites are promising materials for cost-effective printable photovoltaics. Perovskite solar cells with 3.8% power conversion efficiency (PCE) were reported in 2009 by Miyasaka *et al.*,[1] and in just one decade efficiencies have reached 23%.[2] The most widely studied perovskite architype is methylammonium lead iodide ($MAPbI_3$). The use of purified starting materials, in combination with careful optimization of the perovskite fabrication methods, have led to significant improvements in PCE,[2,3] stability and reproducibility of $MAPbI_3$ -based photovoltaic devices.[4–10] The efficiencies of $MAPbI_3$-based devices are currently around 20%.[11–17] Replacing or mixing different cation and anion species in the perovskite lattice often changes the band gap and shifts the charge transporting energy levels, leading to additional device performance.[18–24] Formamidinium lead iodide ($FAPbI_3$), for example, is expected to show improved light harvesting owing to its narrower band gap compared with $MAPbI_3$. However, $FAPbI_3$ undergoes a spontaneous phase transition at room temperature from the photo-active black α-phase perovskite to the photo-inactive yellow δ-phase non-perovskite, making pure $FAPbI_3$ devices less stable.[18,25,26] Fortuitously, Seok *et al.* found that the stability of the α-phase $FAPbI_3$ was increased by adding a small amount of $MAPbBr_3$ into the $FAPbI_3$ to form a mixed composition perovskite.[22] After their work, a variety of perovskites with mixed compositions were developed, and this has grown rapidly into an exciting new trend in perovskite solar cell research. As a recent example, a cesium-containing mixed component perovskite, $Cs_{0.05}(MA_{0.17}FA_{0.83})_{0.95}Pb(I_{0.83}Br_{0.17})_3$, was developed by Saliba *et al.,* which further improves the stability of the α-phase $FAPbI_3$.[23] Rubidium[24] and potassium[27] ions have been used instead of, or in combination with, cesium ions. Solar cells made with these mixed compositions have high efficiencies and good thermal durability, and as a result have come into widespread use as standard perovskite materials.

For the perovskites developed for present work, $FAPbI_3$ derived from $FAPbI_3·2DMF$ complex is used as a purified source of FAI and PbI_2 for perovskites with mixed FA-MA cations. These stable, pure materials provide FAI:PbI_2 components in an exact 1:1 stoichiometry.

The ion ratios of mixed composition perovskites were adjusted to maximize the performance of solar cells. In particular, our interest in the current work is improving the current output of devices using tin(IV) oxide (SnO_2) films as electron transport layers. Recently, SnO_2 has become a popular electron transport layer (ETL), since, unlike titanium(IV) oxide (TiO_2), the films can be grown under low temperature conditions (~150 °C).[28–30] The efficiency of these SnO_2-based devices have tended to be lower than those using mesoporous-TiO_2, although a more efficient example has recently been reported.[31] We predict that by optimizing the composition of mixed perovskites to tune the electronic levels slightly, it should be possible to optimally match the conduction bands of the perovskite with SnO_2 for efficient electron extraction. Varying the ion substitution ratio of I and Br led to the development of a new narrow band gap mixed-component perovskite formulation, $Cs_{0.05}FA_{0.80}MA_{0.15}PbI_{2.75}Br_{0.25}$ (I/Br ratio 11:1), ideally suited to interface with SnO_2 transport layers.

---

[a] Institute for Chemical Research, Kyoto University, Uji, Kyoto 611-0011, Japan
[b] Fine Chemicals R&D, Toda Research Center, Tokyo Chemical Industry Co., Ltd. Toda, Saitama 335-0033, Japan
[c] Institute for Integrated Radiation and Nuclear Science, Kyoto University, Sen-nan-gun, Osaka 590-0494, Japan

†Electronic Supplementary Information (ESI) available: [details of any supplementary information available should be included here]. See DOI: 10.1039/x0xx00000x

Mixed composition materials are known to benefit from annealing at higher temperatures than typically used for $\mathrm{MAPbI_3}$, with 150 °C considered optimal.[29] At this temperature, excess $\mathrm{PbI_2}$ forms on the surface as a result of the partial decomposition of the perovskite.[30] $\mathrm{PbI_2}$ is thought to play a key role in reducing defects in the perovskite film, suppressing the charge carrier recombination processes.[32–34] We confirmed that when the perovskite films were annealed at 150 °C for 5 min or more, $\mathrm{PbI_2}$ gradually appeared on the surface, and that the presence of $\mathrm{PbI_2}$ was found to directly correlate with improvements in the electrical performance of the device. Furthermore, aging in ambient atmosphere (25% relative humidity; RH) for 4–5 days caused a dramatic improvement in device efficiency together with a reduction in the hysteresis of the *J-V* curves. Aging shifted the conduction and valence energy levels in the perovskite layer, and supressed charge carrier recombination in the devices. After aging, highly reproducible solar cells were readily obtained with high output currents and high power conversion efficiencies (maximum ~20.6%).

Results and discussion

Preparation of $\mathrm{FAPbI_3{\cdot}2DMF}$ complex and derivatives

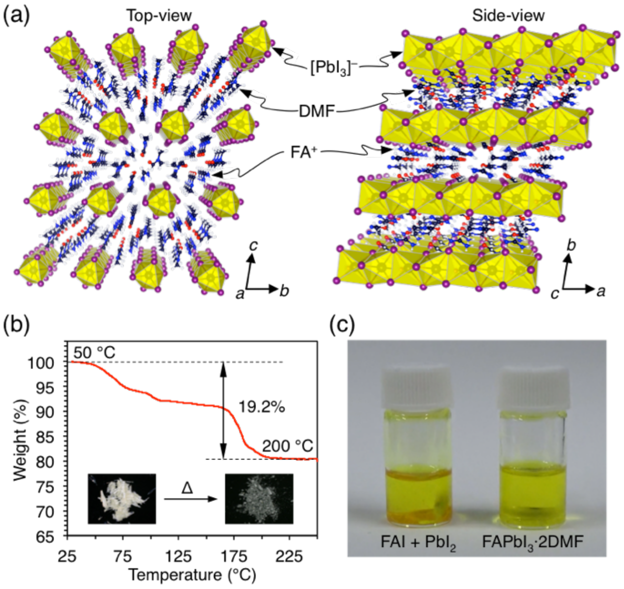

Fig. 1 (a) X-ray crystal structure and (b) TG curve of $\mathrm{FAPbI_3{\cdot}2DMF}$. (c) Comparison of solubility in DMSO between conventional FAI + $\mathrm{PbI_2}$ (left) and $\mathrm{FAPbI_3{\cdot}2DMF}$ (right). Condition: 1.0 M, stirring at 50 °C for 3 min.

$\mathrm{FAPbI_3{\cdot}2DMF}$ complex was obtained by multi-solvent recrystallization in an $\mathrm{N_2}$-filled glovebox, in a similar manner to that of $\mathrm{MAPbI_3{\cdot}DMF}$.[35,36] FAI and $\mathrm{PbI_2}$ (1:1) were dissolved in dry DMF at 70 °C, and the resulting clear yellow solution was transferred to a glass tube. Toluene was layered over the DMF solution. Colorless crystals of $\mathrm{FAPbI_3{\cdot}2DMF}$ were collected after one day. Single-crystal X-ray diffraction (XRD) analysis confirmed that the DMF molecules are intercalated between the octahedral layer of $\mathrm{[PbI_3]^-}$ moieties and the $\mathrm{FA^+}$ cations (Fig. 1a). Solvent loss was meanwhile examined by thermogravimetric analysis (TGA). Results for $\mathrm{FAPbI_3{\cdot}2DMF}$ is given in Fig. 1b. Weight loss began at 50 °C and completed by 200 °C. Over that time, the crystals changed from colorless to black. The total weight loss is 19.2%, while the calculated loss for the removal of two DMF molecules from the structural formula is 18.8%. The product obtained by heating at high temperature is therefore concluded to be $\mathrm{FAPbI_3}$. $\mathrm{FAPbI_3{\cdot}2DMF}$ has good solubility compared with conventional mixture of FAI and $\mathrm{PbI_2}$. $\mathrm{FAPbI_3{\cdot}2DMF}$ dissolves in DMSO in a few minutes at room temperature, more quickly than the corresponding mixture of FAI and $\mathrm{PbI_2}$ (Fig. 1c). Based on trace analysis of 70 elements, the purity of $\mathrm{FAPbI_3{\cdot}2DMF}$ was determined to be 99.998% (Fig. S1), a high value similar to our previously developed purified precursors $\mathrm{PbI_2}$ and $\mathrm{MAPbI_3{\cdot}DMF}$.[35,37,38]

When the $\mathrm{FAPbI_3{\cdot}2DMF}$ crystals were washed with toluene and dried under vacuum, the colorless complex took on a yellow tint. ^{1}H nuclear magnetic resonance (NMR) analysis indicated that the integral ratio of $\mathrm{FA^+}$:DMF was now 1:1 (Fig. S2), while thermogravimetric analysis of the yellow crystalline solids confirmed that the weight loss corresponded to just one molecule of DMF (Fig. S3). Approximately half of the solvent molecules were therefore eliminated from $\mathrm{FAPbI_3{\cdot}2DMF}$ over the course of the washing and drying procedure. Although it is unclear if the solvent ratio is homogenous over the entire crystal, the same 1:1 ratio of $\mathrm{FA^+}$:DMF was confirmed over multiple lots using ^{1}H NMR analysis. The dried material was therefore assigned to the nominal formula $\mathrm{FAPbI_3{\cdot}DMF}$. While this reagent is stable and provides the source of purified $\mathrm{FA^+}$ for the precursor solutions used in the present work, we also confirmed that the remaining intercalated solvent can be removed by drying the complex at 60 °C under vacuum for several days, to give $\mathrm{FAPbI_3}$ as a yellow crystalline solid (δ-phase). The absence of DMF was again confirmed by ^{1}H NMR analysis (Fig. S4). This material is also an excellent precursor for FA-containing mixed composition perovskites, as an alternative to the solvent-intercalated $\mathrm{FAPbI_3{\cdot}DMF}$ (Fig. S5, Table S1.) The $\mathrm{FAPbI_3}$ is stable to long term storage in inert atmosphere (Fig. S4b), in contrast to FAI (Fig. S6).

Iodine-rich mixed composition perovskite with narrow optical gap for $\mathrm{SnO_2}$ ETL-based solar cells

Solar cells made with the mixed composition perovskite, $\mathrm{Cs_{0.05}FA_{0.79}MA_{0.16}PbI_{2.49}Br_{0.51}}$, were previously reported to show high efficiency as well as good durability when used with the standard solar cell device with compact-$\mathrm{TiO_2}$/mesoporous-$\mathrm{TiO_2}$ ETLs.[23] When we attempted to use this composition in devices where the $\mathrm{TiO_2}$ layer was replaced with $\mathrm{SnO_2}$, the current density of the device was limited to about 20 mA cm^{-2}.[39] We therefore began adjusting the composition of perovskites to optimize the energy levels for better compatibility with $\mathrm{SnO_2}$, which has a lower conduction band energy compared to $\mathrm{TiO_2}$. ($\mathrm{TiO_2}$ –4.02 eV, $\mathrm{SnO_2}$ –4.17 eV)[40,41] Somewhat smaller perovskite band gaps should therefore be permissible when using $\mathrm{SnO_2}$ as the electron transport layer. The band gap of $\mathrm{Cs_{0.05}FA_{0.79}MA_{0.16}PbI_{2.49}Br_{0.51}}$ is approximately 1.6 eV, so a narrower gap is expected to increase the device current and the PCE according to the Shottkey-Quessar limit.[42] The band gap of the mixed composition perovskite was adjusted and optimized by varying the I/Br ratio, while keeping the ratio of Cs, MA, and FA approximately constant.

The devices were prepared with the structure: Glass-ITO/SnO_2 (40 nm)/perovskite/2,2′,7,7′-tetrakis(*N*,*N*-di-*p*-methoxyphenylamine)-9,9′-spirobifluorene (spiro-OMeTAD) (200 nm)/Au (80 nm), following the description in the literature.[39] Perovskite precursor solutions were prepared from CsI, MABr, $PbBr_2$, PbI_2, and FAI or $FAPbI_3$·DMF dissolved in DMF:DMSO 3:1 mixed solvent. $FAPbI_3$·DMF was used as the purified FA^+ source. The precursor solutions were deposited on SnO_2–covered ITO substrates by spin-coating. During the spinning, chlorobenzene antisolvent was dripped over the substrate to induce precipitation of the perovskite precursor. The precursor films were annealed on a hot plate at 150 °C. The transition to perovskite is accompanied by a color change in the film from dark-brown to black. The annealing time has a complicated influence of the film morphology, composition, and device performance. As will be shown later, the optimal annealing time was found to be 10 minutes. Four different mixed composition perovskite formulations were evaluated in order to find which I/Br ratio was most suitable to use with SnO_2: $Cs_{0.05}FA_{0.78}MA_{0.12}PbI_{2.49}Br_{0.51}$ (I:Br = 5:1), $Cs_{0.06}FA_{0.84}MA_{0.10}PbI_{2.59}Br_{0.41}$ (I:Br = 6:1), $Cs_{0.05}FA_{0.80}MA_{0.15}PbI_{2.75}Br_{0.25}$ (I:Br = 11:1), and $Cs_{0.05}FA_{0.80}MA_{0.15}PbI_3$ (I:Br = 1:0). The current–voltage (*J*–*V*) curves and incident photon-to-current conversion efficiency (IPCE) spectra of the best devices are shown in Fig. 2a and 2b, respectively, and summarized in Table 1 together with the average values from three cells of each composition. The short circuit current, J_{SC}, increased from 20.8 mA cm^{-2} (I:Br = 5:1), to 22.0 mA cm^{-2} (I:Br = 6:1) , and 23.3 mA cm^{-2} (I:Br = 11:1) as the fraction of iodide ions increased. This was accompanied by a decrease in the open circuit voltage, $V_{OC,}$ however, leaving the PCE almost constant at around 18.5%.). The short circuit current fell slightly to 22.9 mA cm^{-2} for the all-iodine composition (I:Br = 1:0), leading to an overall lower PCE of 17.4 %. The unexpected drop in *J*sc can be attributed to poor film morphology, as these perovskites did not exhibit the same smooth, shiny surface as the other samples (Fig. S7). The IPCE spectra confirmed that the increase in J_{SC} corresponds to a change of the perovskite bandgap. The onset of photo-conversion shifted from 780 nm to 815 nm with increasing iodide content in direct consequence of the narrower optical gap. As the composition with the highest PCE, the perovskite $Cs_{0.05}FA_{0.80}MA_{0.15}PbI_{2.75}Br_{0.25}$ (I:Br = 11:1), was selected for further process optimization of the SnO_2 ETL-based solar cell devices.

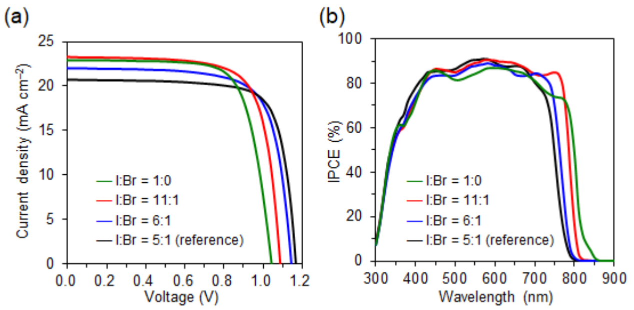

Fig. 2 (a) The *J–V* curves and (b) IPCE spectra of the perovskite solar cells with different I/Br ratios.

Table 1 Photovoltaic parameters of perovskite solar cells with different I/Br ratios

I:Br ratio	J_{SC} (mA cm^{-2})	V_{OC} (V)	FF	PCE (%)
1:0 Best	22.9	1.04	0.73	17.4
1:0 Avg.	22.8±0.08	1.05±0.005	0.73±0.009	17.3±0.2
11:1 Best	23.3	1.09	0.74	18.6
11:1 Avg.	23.2±0.08	1.08±0.004	0.73±0.002	18.5±0.2
6:1 Best	22.0	1.15	0.73	18.5
6.1 Avg.	22.0±0.03	1.14±0.005	0.73±0.002	18.3±0.2
5:1 Best	20.8	1.17	0.76	18.5
5:1 Avg.	20.7±0.04	1.16±0.004	0.76±0.006	18.2±0.3

Neutron analysis of the perovskite composition

For mixed composition perovskites, there is always a concern that the perovskite might have a different composition from a concentration ratio of the precursor solution. It is therefore important to confirm the composition ratio in the perovskite film prepared by the above method. Since the heavy elements Cs, I, and Br ions cannot be easily observed by NMR spectroscopy, we instead confirmed the I/Br ratio in the sample prepared using the purified $FAPbI_3$·DMF complex by neutron activation analysis (NAA) at the Kyoto University Reactor (KUR) facility (additional information given in the Supporting Information). The results indicated the composition of $Cs_{0.08}(FA+MA)_{0.92}PbI_{2.78}Br_{0.22}$, in close agreement with the component ratio of the precursor solution as $Cs_{0.05}FA_{0.80}MA_{0.15}PbI_{2.75}Br_{0.25}$. The I/Br ratio is comparable to the ratio of the precursor solution used to prepare the perovskite samples.

Annealing optimization for iodide-rich mixed component $Cs_{0.05}FA_{0.80}MA_{0.15}PbI_{2.75}Br_{0.25}$ perovskites

The mixed composition perovskites were generally found to be relatively easy materials to work with at the spin-coating stage. Using the solvent engineering method with antisolvent dripping, flat and smooth films were readily obtained on SnO_2-

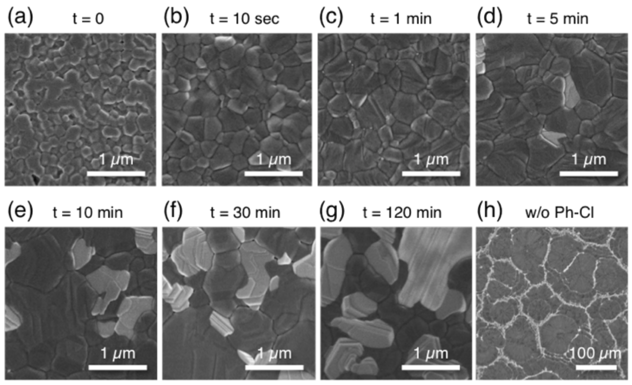

Fig. 3 Top-view SEM images of the perovskite films prepared by different annealing time. The films were annealed at 150 °C for (a) 0 s, (b) 10 s, (c) 1 min, (d) 5 min, (e) 10 min, (f) 30 min, and (g) 120 min. Film (h) was annealed for 10 minutes, but fabricated without antisolvent addition step.

covered ITO substrates. Since the wet film fabrication process seemed to already be broadly effective, we focused instead on optimizing the thermal annealing step. We investigated the effect of the annealing time on the quantity of PbI_2 that formed on the perovskite layer and measured the corresponding change in device performance for solar cells prepared under the same conditions. Fig. 3 shows the top-view SEM images of the perovskite films annealed at 150 °C for between 10 s and 120 min. The as-spun precursor film has a granular morphology (Fig. 3a). After a very short annealing time of approximately 10 s, the film changed to a flat and tightly packed layer (Fig. 3b). As seen in Fig. 3c-g, the quantity of high brightness material increased with annealing time. This material was confirmed by energy dispersive X-ray spectroscopy (EDX) and transmission electron microscope (TEM) analysis to be PbI_2 (Fig. S8-S10). At the early stage of the annealing, within 5 min, only the grain ripening of the main perovskite film was observed, with no or little formation of PbI_2. In order to extract significant quantities of PbI_2, it is necessary to anneal the film at 150 °C for 5 minutes or more. Next, we confirmed a positive correlation of the device performance with the quantity of the PbI_2 formed on the perovskite surface. Devices were prepared with perovskite layers annealed for 1, 5, 10, and 30 min. *J*–*V* curves and IPCE spectra are presented in Fig. S11 and Table S2. The annealing time of 10 min was found to give the best device efficiency, though there was only modest variation between the results on 5 and 30 min.

Aging effects of air-exposed devices

In this section, the aging effect will be discussed using $Cs_{0.05}FA_{0.80}MA_{0.15}PbI_{2.75}Br_{0.25}$ as the standard mixed component perovskite and 150 °C for 10 min as the optimized annealing method. The passivation effect of excess PbI_2 at the perovskite interfaces is widely known[33,34], and it has been shown that air aging under dark conditions improved the charge carrier diffusion length of mixed-halide perovskite films.[43] While

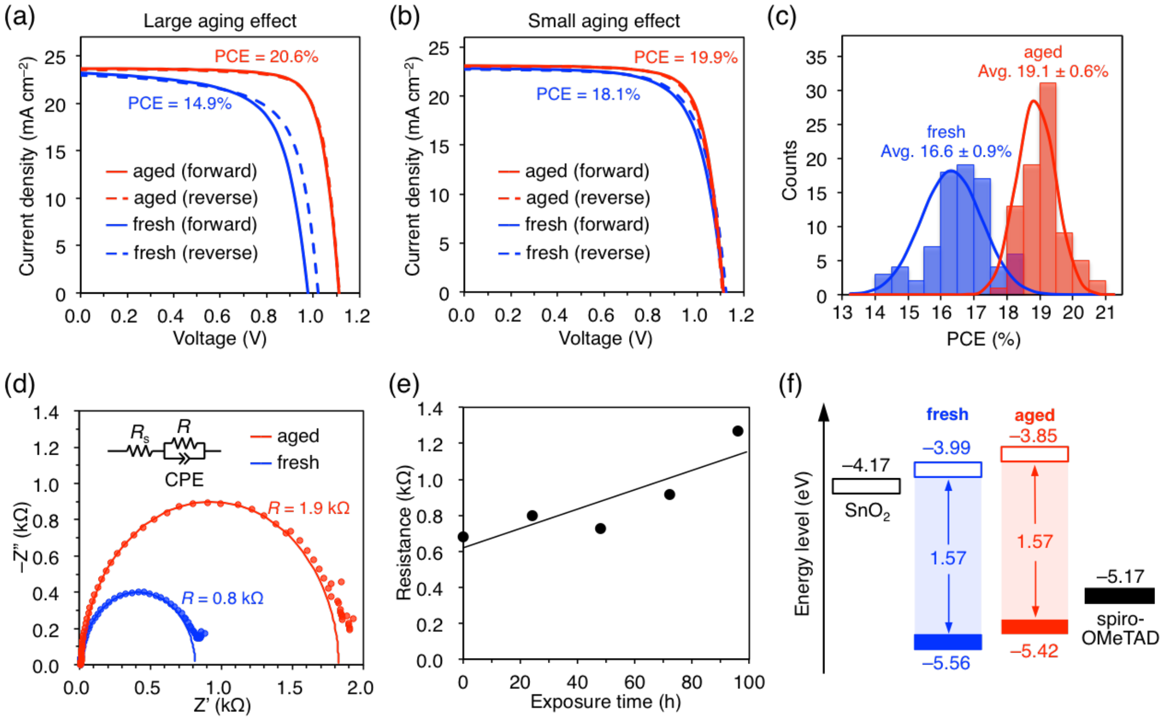

Fig. 4 *J*–*V* curves for a $Cs_{0.05}FA_{0.80}MA_{0.15}PbI_{2.75}Br_{0.25}$ (I/Br ratio 11:1) device showing (a) a large aging effect and (b) a small aging effect. (c) The PCE distribution of 80 cells, and (d) complex impedance plots of the perovskite solar cells as fresh (blue) and aged for 4 d (red). (e) The average recombination resistance for 11 devices as a function of aging time. (f) Energy diagrams of the perovskite before and after aging, together with SnO_2 and spiro-OMeTAD.

Table 2 Photovoltaic parameters of $Cs_{0.05}FA_{0.80}MA_{0.15}PbI_{2.75}Br_{0.25}$ (I/Br ratio 11:1) perovskite solar cells for various aging effects

		J_{SC} (mA cm^{-2})	V_{OC} (V)	FF	PCE (%)	R_s (Ω cm^2)	R_{sh} (Ω cm^2)
Large aging effect	fresh	23.2	0.98	0.66	14.5	4.0	626
	aged	23.7	1.11	0.78	20.6	5.0	2635
Small aging effect	fresh	23.0	1.10	0.72	18.1	6.4	3046
	aged	23.3	1.11	0.77	19.9	5.4	3414
Average of all devices	fresh	22.9 ±0.21	1.07 ±0.04	0.68 ±0.02	16.6 ±0.9	5.6 ±0.9	1713 ±775
	aged	23.1 ±0.20	1.09 ±0.02	0.76 ±0.01	19.1 ±0.6	4.9 ±0.7	5057 ±1543

examining the durability and reproducibility of the solar cells, we noticed that the performance of devices dramatically improved after being stored in the air (25% RH) without encapsulation for 4–5 days. This aging effect is demonstrated in Fig. 4a, showing the *J*–*V* curves for the device which exhibited the greatest improvement. The PCE was 14.5% in the fresh state and increased to 20.6% after aging. In contrast, Fig. 4b shows the *J*–*V* curves for a device which exhibited a minimal aging effect. The average PCE of 80 devices increased from 16.6 ± 0.9% to 19.1 ± 0.6% (Fig. 4c). The performance results are summarized in Table 2. It should also be noted that hysteresis in the *J*–*V* curves becomes negligible after aging (Fig. 4a,b). Although $MAPbI_3$ quickly degrades in humid air to form PbI_2, mixed composition perovskites are stable for up to a month in similar conditions.[43] While aging effects in mixed composition devices cannot be directly attributed to an increase in the quantity of PbI_2 over time, as this is largely set by the annealing conditions, perovskite layers annealed to give significant excess of surface PbI_2 gave the best performance after aging. Examining the complex impedance plots of the fresh and aged devices, obtained under AM1.5G and 0 V applied bias (Fig. 4d), both showed near-ideal single semicircular curves, with a small offset at the origin corresponding to the series resistance, R_s, of the device. The size of the semicircle relates to the primary shunt resistance, R_{sh}, which is generally taken as defining a recombination resistance when the device is measured under strong illumination.[44] In the device which showed the most improvement by aging, the recombination resistance increased from 0.8 kΩ to 1.9 kΩ, reflecting the reduction in charge carrier recombination events in the device. While it is well known that the conductivity of spiro-OMeTAD improves its conductivity on air oxidation,[45,46] no indication of a significant series resistance was detected in the complex impedance plot of the fresh device. The improved device performance may instead be framed in terms of the charge extraction efficiency at the interface between the spiro-OMeTAD layer and the perovskite surface, and the influence of the excess PbI_2 which formed at that interface during annealing. We speculate that the changes result from water vapour in the air slowly reacting with the PbI_2. The average recombination resistance of the 11 tested devices increased as a direct function of the aging time (Fig. 4e). Charge extraction is also influenced by the energy level alignment. We confirmed that after aging, the energy levels of the valence and conduction band of the perovskite layer shifted with respect to the vacuum level. Photoemission spectroscopy (PES) measurements revealed that the valence band of the perovskite increased from –5.56 eV to –5.42 eV, while the band gap remained unchanged (Fig. 4f, S12).

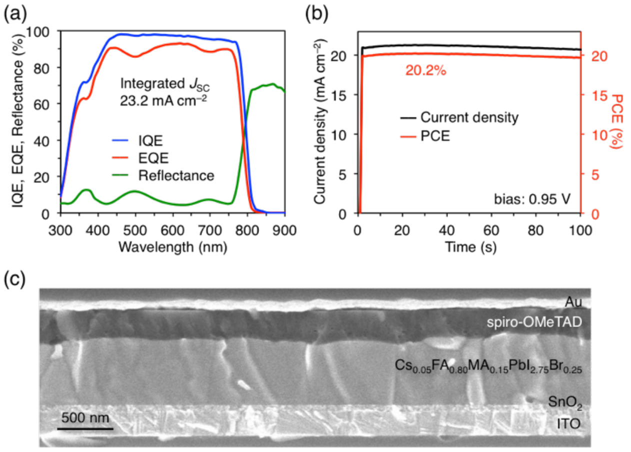

Fig. 5 (a) IQE (blue line), EQE (red line), and reflectance spectra (green line) as well as (b) stabilized current density (black line) with stabilized power output (red line), and (c) cross-sectional SEM image of the best performing device.

The internal quantum efficiencies (IQE) and external quantum efficiencies (EQE) as well as reflectance spectra of the best performing cell (PCE = 20.6%) are shown in Fig. 5a. The integrated J_{SC} from the EQE was estimated to be 23.2 mA cm^2, comparable with the values obtained in the *J*–*V* measurement. The current onset occurred at above 800 nm (< 1.55 eV), in close agreement with the optical gap (1.57 eV). The average EQE and IQE over the range of 450 - 750 nm was 90% and 98%, respectively. Fig. 5b shows the stabilized power output (SPO) and current density of the best performing device over time, recorded at a fixed applied voltage of 0.95 V. A maximum SPO of 20.2% was observed after 30 s recording. Finally, the cross-sectional SEM image is shown in Fig. 5c, confirming that the device fabricated under the optimized conditions produced a flat and dense perovskite layer, with excellent grain morphology.

Conclusions

A new iodine-rich formulation, $Cs_{0.05}FA_{0.80}MA_{0.15}PbI_{2.75}Br_{0.25}$, (I/Br ratio 11:1) was introduced which gave optimal compatibility with SnO_2 electron transport layers. Adjusting the I/Br ratio expanded the absorption region to longer wavelengths. We confirmed that segregation of PbI_2 during high temperature annealing improved device performance and we determined the optimal annealing time needed to produce effective quantities of PbI_2. The performance of the perovskite solar cells was dramatically and reproducibly enhanced by exposure to ambient atmosphere over several days, and correlated with a shift of the charge transporting energy levels of the perovskite and a significant reduction in charge carrier recombination events. Combining these optimizations – optical gap tuning, optimized annealing time, and device aging – solar cell devices with a high power conversion efficiency up to 20.6% could be reliably obtained.

Author contributions

A. Wakamiya conceived the study. M. Ozaki, Y. Murata, R. Murdey and A. Wakamiya wrote the manuscript. M. Ozaki, Y. Ishikura, M. A. Truong, J. Liu and R. Murdey performed the experiments and analysis of the results on the solar cells; I. Okada and T. Tanabe contributed the analysis of the purity of materials, while the neutron activation analysis (NAA) was done by S. Sekimoto and T. Otsuki at the Kyoto University Reactor (KUR) facility. All authors contributed to the discussion of the results and the manuscript editing.

Conflicts of interest

There are no conflicts to declare.

Acknowledgements

This study was partially supported by the COI (JPMJCE 1307), ALCA (JPMJAL 1603), and ERATO (JPMJER 1302) programs from the Japanese Science and Technology Agency (JST), NEDO, and Grant-in-Aid for JSPS Fellows (Grant Number 18F18342). We would like to thank Prof. Kazunari Matsuda, Prof. Toshiharu Teranishi, Dr. Ryota Sato, and Dr. Tokuhisa Kawawaki (Kyoto University) for advice on the measurement of SEM images, and Dr. Tsukasa Koyama, Mr. Sumihisa Ishikawa, Mr. Kentaro Kato, and Mr. Takahiro Harada (Toray Research Center Inc.) for EDX and TEM analysis, and Prof. Takahiro Sasamori (Nagoya City University) for advice on the single-crystal X-ray diffraction analysis.

References

1 A. Kojima, K. Teshima, T. Shirai, T. Miyasaka, *J. Am. Chem. Soc.,* 2009, **131**, 6050–6051.
2 Best Research Cell Efficiencies Chart. National Renewable Energy Laboratory (NREL), 2019.
3 M. A. Green, Y. Hishikawa, E. D. Dunlop, D. H. Levi, J. Hohl-Ebinger, M. Yoshita, A. W. Y. Ho-Baillie, *Prog. Photovolt. Res. Appl.,* 2019, **27**, 3–12.
4 M. M. Lee, J. Teuscher, T. Miyasaka, T. N. Murakami, H. J. Snaith, *Science,* 2012, **338**, 643–647.
5 J.-H. Im, I.-H. Hang, N. Pellet, M. Grätzel, N.-G. Park, *Nat. Nanotechnol*., 2014, **9**, 927–932.
6 J. Burschka, N. Pellet, S.-J. Moon, R. Humphry-Baker, P. Cao, M. K. Nazeeruddin, M. Grätzel, *Nature,* 2013, **499**, 316–319.
7 M. Liu, M. B. Johnston, H. J. Snaith, *Nature,* 2013, **501**, 395–398.
8 Q. Chen, H. Zhou, Z. Hong, S. Luo, H.-S. Duan, H.-H. Wang, Y. Liu, G. Li, Y. Yang, *J. Am. Chem. Soc.,* 2014, **136**, 622–625.
9 N. J. Jeon, J. H. Noh, Y. C. Kim, W. S. Yang, S. Ryu, S. I. Seok, *Nat. Mater.,* 2014, **13**, 897–903.
10 M. Xiao, F. Huang, W. Huang, Y. Dkhissi, Y. Zhu, J. Etheridge, A. Gray-Weale, U. Bach, Y.-B. Cheng, L. Spiccia, *Angew. Chem., Int. Ed.,* 2014, **53**, 9898–9903.
11 N. Ahn, D. Son, I. Jang, S. M. Kang, M. Choi, N. Park, *J. Am. Chem. Soc.,* 2015, **137**, 8696–8699.
12 Q. Wang, Q. Dong, T. Li, A. Gruverman, J. Huang, *Adv. Mater.,* 2016, **28**, 6734–6739.
13 C. Momblona, L. Gil-Escrig, E. Bandiello, E. M. Hutter, M. Sessolo, K. Lederer, J. Blochwitz-Nimoth, H. J. Bolink, *Energy Environ. Sci.,* 2016, **9**, 3456–3463.
14 J. Zhao, X. Zheng, Y. Deng, T. Li, Y. Shao, A. Gruverman, J. Shield, J. Huang, *Energy Environ. Sci.,* 2016, **9**, 3650–3656.
15 W. S. Yang, J. H. Noh, N. J. Jeon, Y. C. Kim, S. Ryu, J. Seo, S. I. Seok, *Science,* 2015, **348**, 1234–1237.
16 C. Roldán-Carmona, P. Gratia, I. Zimmermann, G. Grancini, P. Gao, M. Grätzel, M. K. Nazeeruddin, *Energy Environ. Sci.,* 2015, **8**, 3550–3556.
17 H. D. Kim, H. Ohkita, H. Benten, S. Ito, *Adv. Mater.,* 2016, **28**, 917–922.
18 L. K. Ono, E. J. Juarez-Perez, Y. Qi, *ACS Appl. Mater. Interfaces*, 2017, **9**, 30197–30246.
19 J. H. Noh, S. H. Im, J. H. Heo, T. N. Mandal, S. I. Seok, *Nano Lett.,* 2013, **13**, 1764–1769.
20 O. J. Weber, B. Charles, M. T. Weller, *J. Mater. Chem. A,* 2016, **4**, 15375–15382.
21 T. M. Koh, K. Fu, Y. Fang, S. Chen, T. C. Sum, N. Mathews, S. G. Mhaisalkar, P. P. Boix, T. Baikie, *J. Phys. Chem. C,* 2014, **118**, 16458–16462.
22 N. J. Jeon, J. H. Noh, W. S. Yang, Y. C. Kim, S. Ryu, J. Seo, S. I. Seok, *Nature,* 2015, **517**, 476–480.
23 M. Saliba, T. Matsui, J.-Y. Seo, K. Domanski, J.-P. Correa-Baena, M. K. Nazeetuddin, S. M. Zakeeruddin, W. Tress, A. Abate, A. Hagfeldt, M. Grätzel, *Energy Environ. Sci.,* 2016, **9**, 1989–1997.
24 M. Saliba, T. Matsui, K. Domanski, J.-Y. Seo, A. Ummadisingu, S. M. Zakeeruddin, J.-P. Correa-Baena, W. R. Tress, A. Abate, A. Hagfeldt, M. Grätzel, *Science,* 2016, **354**, 206–210.
25 F. Ma, J. Li, W. Li, N. Lin, L. Wang, J. Qiao, *Chem. Sci.,* 2017, **8**, 800–805.
26 J. S. Yun, J. Kim, T. Young, R. J. Patterson, D. Kim, J. Seidel, S. Lim, M. A. Green, S. Huang, A. Ho-Baillie, *Adv. Funct. Mater.,* 2018, **28**, 1705363.
27 Z. Tang, T. Bessho, F. Awai, T. Kinoshita, M. M. Maitani, R. Jono, T. N. Murakami, H. Wang, T. Kubo, S. Uchida, H. Segawa, *Sci. Rep.,* 2017, **7**, 12183.
28 L. Xiong, Y. Guo, J. Wen, H. Liu, G. Yang, P. Qin, G. Fang, *Adv. Funct. Mater.,* 2018, **28**, 1802757.
29 Q. Jiang, L. Zhang, H. Wang, X. Yang, J. Meng, H. Liu, Z. Yin, J. Wu, X. Zhang, J. You, *Nat. Energy,* 2016, **2**, 16177.
30 Q. Jiang, Z. Chu, P. Wang, X. Yang, H. Liu, Y. Wang, Z. Yin, J. Wu, X. Zhang, J. You, *Adv. Mater.,* 2017, **29**, 1703852.
31 Q. Jiang, Y. Zhao, X. Zhang, X. Yang, Y. Chen, Z. Chu, Q. Ye, X. Li, Z. Yin, J. You, *Nat. Photonics*, 2019, DOI 10.1038/s41566-019-0398-2.
32 Q. Chen, H. Zhou, T.-B. Song, S. Luo, Z. Hong, H.-S. Duan, L. Dou, Y. Liu, Y. Yang, *Nano Lett.,* 2014, **14**, 4158–4163.
33 D. H. Cao, C. C. Stoumpos, C. D. Malliakas, M. J. Katz, O. K. Farha, J. T. Hupp, M. G. Kanatzidis, *APL Mater.,* 2014, **2**, 091101.
34 T. J. Jacobsson, J.-P. Correa-Baena, E. H. Anaraki, B. Philippe, S. D. Stranks, M. E. F. Bouduban, W. Tress, K. Schenk, J. Teuscher, J.-E. Moser, H. Rensmo, A. Hagfeldt, *J. Am. Chem. Soc.,* 2016, **138**, 10331–10343.
35 A. Wakamiya, Y. Hirose, A. Shimazaki, Patent PCT/JP2016/087529.
36 M. Ozaki, A. Shimazaki, M. Jung, Y. Nakaike, N. Maruyama, S. Yakumaru, A. I. Rafieh, T. Sasamori, N. Tokitoh, P. Ekanayake, Y. Murata, R. Murdey, A. Wakamiya, *Angew. Chem. Int. Ed.* 2019, DOI 10.1002/anie.201902235 *(in press)*
37 https://www.tcichemicals.com/eshop/ja/jp/commodity/L0279/.
38 A. Wakamiya, M. Endo, T. Sasamori, N. Tokitoh, Y. Ogomi, S. Hayase, Y. Murata, *Chem. Lett.,* 2014, **43**, 711–713.
39 F. Yang, J. Liu, H. E. Lim, Y. Ishikura, K. Shinokita, Y. Miyauchia, A. Wakamiya, Y. Murata, K. Matsuda, *J. Phys. Chem.,* 2018, **122**, 17088–17095.
40 J. P. C. Baena, L. Steiier, W. Tress, M. Saliba, S. Neutzner, T. Matsui, F. Giordano, T. J. Jacobsson, A. R. S. Kandada, S. M. Zakeeruddin, A. Petrozza, A. Abate, M. K. Nazeeruddin, M. Grätzel, A. Hagfeldt, *Energy Environ. Sci.,* 2015, **8**, 2928–2934.
41 H. Wang, H. Yu, W. Xu, Z. Yuan, Z. Yan, C. Wang, X. Liu, M. Fahlman, J.-M. Liu, X.-K. Liu, F. Gau, *J. Mater. Chem. C,* 2018, **6**, 6996–7002.
42 W. Shockley, H. J. Queisser, *J. Appl. Phys.,* 1961, **32**, 510–519.
43 G.W.P. Adhyaksa, L.W. Veldhuizen, Y. Kuang, S. Brittman, R.E.I. Schropp, and E.C. Garnett, *Chem. Mater.,* 2016, **28**, 5259-5263.
44 A. Dualeh, T. Moehl, N. Tétreault, J. Teuscher, P. Gao, M. K. Nazeeruddin, M. Grätzel, *ACS Nano,* 2014, **8**, 362–373.

45 A. Abate, T. Leijtens, S. Pathak, J. Teuscher, R. Avolio, M. E. Errico, J. Kirkpatrik, J. M. Ball, P. Docampo, I. McPherson, H. J. Snaith, *Phys. Chem. Chem. Phys.,* 2013, **15**, 2572–2579.

46 W. H. Nguyen, C. D. Baile, E. L. Unger, M. D. McGehee, *J. Am. Chem. Soc.,* 2014, **136**, 10996–11001.